PAPER

Check for updates

An insight into battery degradation for the proposal of a battery-friendly charging technique†

Bikash Sah [ID] and Praveen Kumar*

Lithium-ion batteries have become popular for electric vehicles due to their exceptional ability to deliver a high specific power and energy density. However, one of the main drawbacks of these batteries is the inevitable capacity fading that results from degradation over time. The rate at which the capacity of Li-ion batteries fades in EVs is highly dependent on various factors, such as the charging rate, fluctuations in the internal cell temperature, the external ambient temperature, and the driving patterns of the user. Determining the root cause of degradation and constraining its rate in Li-ion batteries, which occurs due to electrochemical processes, remains challenging. This is due to the complex interplay between chemical, electrical, and mechanical parameters that influence the degradation process. The authors of this study have sought to shed light on the causes of degradation by examining the variations in parameters across multiple charge types and rates at different ambient temperatures. While previous research has proposed several charging algorithms aimed at resolving the degradation issue in Li-ion batteries, there is still a need for a unified technique that can effectively constrain the degradation rate at any ambient temperature. This approach should consider the electrochemical phenomena within the battery, grid conditions, and user requirements. The authors of this study have proposed a new battery-friendly charging scheme, which is suitable for the rapid charging of batteries at various ambient temperatures and is effective in mitigating degradation. The study also suggests the suitability of different charging techniques for energy-intensive or power-intensive applications, to provide a comprehensive and systematic approach to developing a new charging technique.

1 Introduction

Lithium-ion batteries have shown promising characteristics to meet the requirements of both hybrid and battery electric vehicles. Lithium-ion batteries were first commercialised in 1991 by the Sony Corporation.[1] The higher energy density, specific energy and power density of Li-ion batteries are a few primary reasons for their wider utilisation as energy storage devices in EVs. The equivalent weight of the lithium metal compound (160 g Li kW^{-1} h^{-1}) used in the battery's negative electrode is low compared with other chemistries of secondary batteries.[2] The size of the positive lithium ion (0.74 Å) is also very small, providing ease of diffusion and efficient intercalation and deintercalation of Li$^+$ ions in the electrodes of the battery. The lower weight of Li metal leads to a higher energy density and specific energy, and the size of its ion helps to increase the power density of the batteries. So far, researchers

have proposed a variety of lithium-ion chemistries that have either been commercialised or are still under research.[1,3] The ongoing research in batteries for application in EVs aims to improve the safety, thermal stability, energy density, rate of charge acceptance and cycle durability, and to reduce the manufacturing and environmental cost.[4,5]

Although Li-based chemistry is commercially used in EVs, it has limitations that hinder its acceptance. The Li compounds and the materials required for manufacturing Li-ion batteries should be free from impurities. Furthermore, metals such as lithium, nickel, cobalt and manganese are costly. Hence, the development and manufacturing processes of Li-ion batteries are high.[6]

1.1 Capacity fading

Capacity fade due to ageing and the change in the battery rate due to variation of the ambient temperature are the major issues related to Li-ion batteries. Calendar and cyclic ageing are the two types of ageing that are characterised in batteries. Calendar ageing is linked to the storage conditions of batteries, the state of charge (SoC), and the ambient temperature of the storage area. A higher storage temperature and SoC instigates secondary reactions.[7] By contrast, cyclic ageing is characterised

*Electric Mobility Lab, Department of Electronics and Electrical Engineering, Indian Institute of Technology Guwahati, India. E-mail: praveen_kumar@iitg.ac.in;
Fax: +91-361-2582542; Tel: +91-361-258-2525*

by degradation in the battery due to the charge–discharge cycle. Structural changes in the electrodes, the formation of a solid electrolyte layer, chemical decomposition or dissolution, and lithium plating are a few resultants of cyclic ageing.[8] The capacity fade of Li-ion batteries is a widely researched topic in the literature.[9] The literature highlights that the magnitude and pattern of the applied current density, the ambient and internal temperature of the battery, and packaging and mechanical stress have a major role in deciding the rate of capacity fade.[10] The discharge pattern of the batteries also impacts the capacity fade. However, the discharge pattern in an EV is based on the current requirement to drive the motor in the powertrain. Hence, instead of studying capacity fade due to discharge patterns in an EV, the sizing and efficiency improvement of entities in a powertrain are widely studied.

The research directions of capacity fade are diverse. Research into electrodes (material, structure, chemistry and binders), electrolytes (chemistry and additives), the structure of the battery, tabs, parameter estimation, electrochemical modelling, mechanical modelling, the causes of capacity fade, electrical modelling and charging techniques are commonly found in the literature.[10,11] However, they have a common question: how can the battery be charged at the fastest possible rate with minimum capacity fade? Rapid charging and low capacity fade are opposing goals, as shown in Fig. S6 (ESI†), which shows the increase in the rate of capacity fade with an increase in the charging rate. An increase in the charging rate corresponds to a decrease in the time to charge.

Furthermore, the battery is an electrochemical system. Hence, it requires more profound insights into the chemical and mechanical changes that occur inside the battery to understand the causes of capacity fade. Chemical and mechanical

degradation are the two types of degradation reported in the literature.

The processes of chemical and mechanical degradation and their dependency on the charging techniques as well as the ambient temperature have been described in the literature. However, there is a lack of studies that provide a deeper insight by describing the variations in chemical and mechanical parameters of the batteries with changes in the charging technique. The parameters studied widely in the literature are the inactive material, SEI layer thickness, loss of capacity due to lithium plating, overpotential, lithiation, porosity, tortuosity, and particle crack length.[10,12–17] The formation and growth of the SEI layer, lithium plating, and the loss of lithium due to electrolytic reactions have been reported as major causes of lithium loss.[17] The variation of these studied parameters results in a change in the capacity, charging time, energy and power.[13,18] Moreover, the above parameters are dependent on the ambient temperature of the battery. Studies related to the impact on the battery parameters with changes in the ambient temperature and charging technique are also missing from the literature.

Hence, via this work, the authors describe the impact of C_{rate} on the rate of chemical and mechanical degradation, the suitability of charging techniques at different ambient temperatures, and the suitability of the charging techniques for high-power and low-power applications. Furthermore, for the first time, a commercially feasible and practically implementable novel charging technique that is suitable for all applications and ambient temperatures, considering the user's requirements and conditions of the electric grid, is proposed for rapid charging with constrained degradation.

Fig. 1 shows the structure of a lithium-ion battery, which comprises two electrodes, an electrolyte and a porous
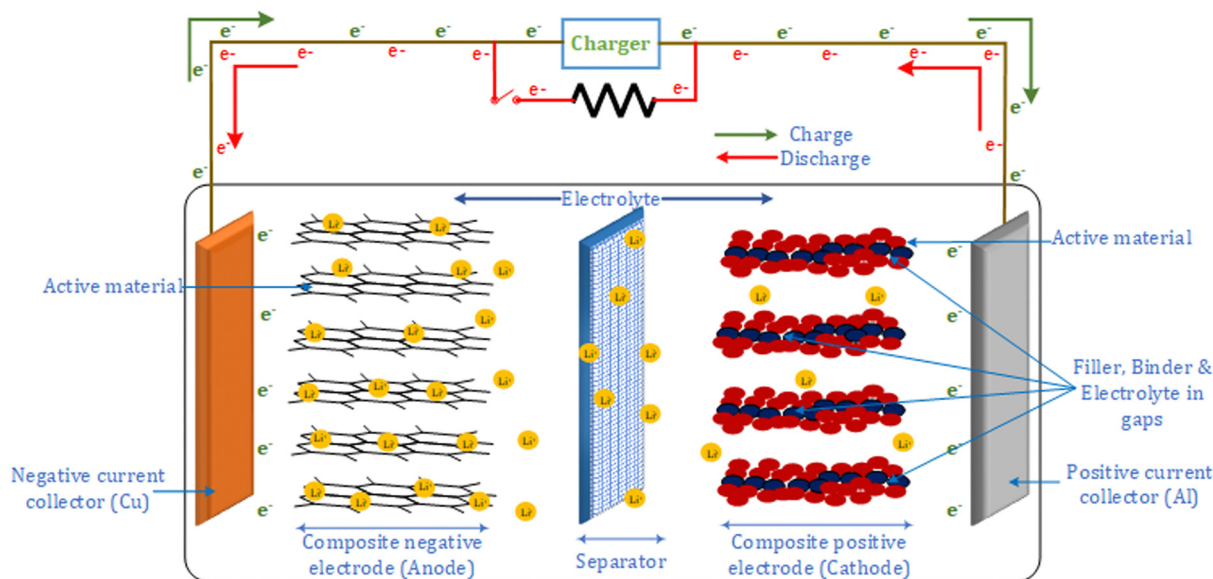
Fig. 1 Model of the battery with all components depicting the process of charging and discharging using the direction of flow of electrons. The arrows and electrons in red depict the discharging process, whereas those in green depict the charging process. The electrons flow *via* the connecting wires, and the positive ions diffuse to either electrode (positive or negative) depending on the process of charging and discharging *via* the electrolyte.

© 2023 The Author(s). Published by the Royal Society of Chemistry

separator. The electrodes are made using active material particles held together using binders, and their structure helps in storing lithium. Current collectors are connected to the electrodes for electrical connection. The direction of the lithium-ion flow determines the charge and discharge in the battery. During discharge, the intercalated lithium in the negative electrode diffuses to the surface, initiating an electrochemical reaction. Each electrochemical reaction leads to the release of a Li^+ ion and an electron. The electrolyte prevents the flow of electrons but allows the Li^+ ion to diffuse towards the positive electrode. Hence, the electrons *via* the electrode and current collector travel to the positive electrode. At the surface of the positive electrode, the Li^+ ion combines with the electron to form a lithium atom, which is intercalated between the positive electrode particles. The process is reversed in the case of charging.

Apart from the required electrochemical reactions for charging and discharging, lithium-ion batteries undergo various undesirable reactions known as secondary or side reactions. These secondary reactions are a major reason for battery degradation.[19] The amplitude, frequency, and time to charge or discharge impact the rate of secondary reactions, leading to two types of degradation mechanism: chemical and mechanical. Furthermore, the temperature and states of the battery also impact the rate of either degradation mechanism. Chemical degradation dominates at a lower applied current at a normal ambient temperature, while a higher applied current and a higher ambient temperature lead to fast mechanical degradation.[20,21] Hence, changing the current pattern while charging is often explored to reduce the degradation of batteries.

1.2 Charging techniques reported in literature

Fig. 2 shows the different types of charging proposed in the literature for rapid charging and control over the degradation of the battery. The charging techniques can be classified into conventional, active control, sinusoidal ripple, boost, constant temperature–constant voltage (CT–CV) and model-based charging. Each type of charging technique is proposed to increase the charging efficiency, reduce the charging time, and reduce battery degradation compared with conventional techniques (mostly CC–CV).

Constant current (CC) was the first technique used to charge the battery. The battery is considered to be fully charged when charging at a constant current leads to an increase in the terminal voltage to a fixed cut-off value. Since the battery is an electrochemical system, it experiences a reduction in the open-circuit voltage after turn-off. Hence, a new constant current–constant voltage (CC–CV) technique was proposed in which the battery is charged using a fixed current value up to the specified cut-off voltage using a constant current.[22,23] On reaching the cut-off voltage, the CV gets activated, in which the voltage is kept constant, and the current starts to reduce. At a specified current value (50 mA), the battery is considered to be fully charged.[24] The reduction in current in the case of CV significantly increases the charging time. However, it allows the settling of mass and ions in the battery, helping to reduce the concentration gradients within the electrode and leading to greater energy storage for a specified maximum voltage. The simplicity of implementing CC–CV and its ability to transfer more energy to the battery has made it a standard charging protocol.[25]

Researchers further exploited the idea of settling ions or mass in the battery *via* pulse charging. During the pulse-charge method, the continuous current is interrupted periodically to give rest phases, or discharge pulses.[26,27] These rest phases and discharge pulses help to settle the kinetics of ions and compounds in the battery. Three types of pulse charging have been reported in the literature: pulse charging without discharge, pulse charging with different current amplitude stages, and
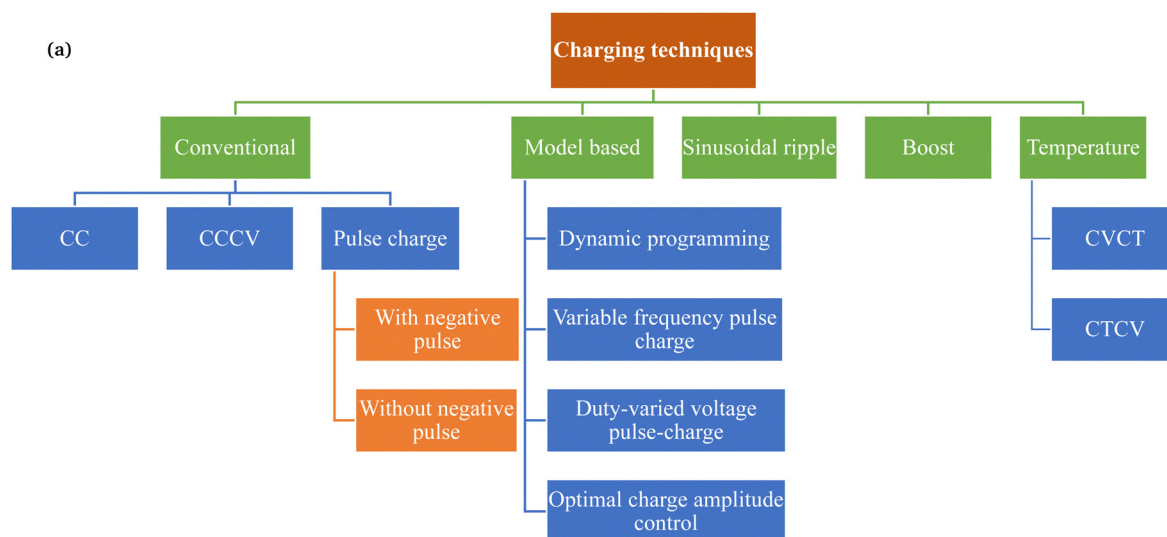

Fig. 2 Types of charging techniques reported in the literature and a few typical current and voltage waveforms; all the types of charging reported in the literature are extensively reviewed and classified appropriately.

pulse charging with short discharge pulses.[28,29] The rest and discharge phases aim to reduce the following: (a) the mechanical stress in the electrode particles due to uneven insertion and extraction of lithium in the solid particles, and (b) the possibility of the electrochemical potential at the anode becoming negative, with concentration polarisation. Research has shown other benefits, such as the inhibition of dendrite formation in the battery, better charging and discharging efficiencies, and active material utilisation.[30]

Reports in the literature have shown that the application of a high current when the battery is at a state of high open-circuit voltage (OCV) and high SoC accelerates battery degradation due to the increased intercalation of Li$^+$ ions in the electrodes and side reactions in the surrounding region of the electrodes in a battery.[12] However, at the state of low OCV and SoC, the battery can be charged at a high current. Hence, Notten *et al.* proposed a charging technique called boost charging.[31] Boost charging is characterised by a high charge current (1C) for a short period that leads to a fast charge of up to one-third of the battery capacity. After that, conventional controlled low current CC–CV is used to charge the remaining capacity. Although boost charging results in a fast charge with controlled degradation, its implementation is challenging because of the unknown high current that flows into the battery due to the high voltage at the charger terminals. Moreover, temperature-increase and degradation studies have not yet been well discussed in the literature for boost charging. Compared with other charging techniques such as CC–CV, boost charging is able to input more charge in the battery, as recorded during the initial fast charge period. However, the rise in the battery temperature during the boost charge has been another challenge.[27,31,32] The increased rate of charge transfer accelerates the process of intercalation. Since the movement of ions is limited by the viscosity of the electrolyte and the porosity of the electrodes, the resistance to the movement of ions increases the temperature of the cell.

Numerous studies have shown a rise in temperature with an increase in the number of charge–discharge cycles. The temperature rise in the battery is due to an increase in the impedance or the chemical kinetics upon the application of a high current for charging or both.[24] Hence, considering the impact of temperature on ageing, Hu *et al.* analysed a new type of charging protocol, *i.e.*, constant voltage constant temperature (CVCT) using the electro-thermal-ageing model.[33] The analysis showed a tradeoff between the charge time and the ageing of the battery. The constant temperature constant voltage (CTCV) charging protocol is another technique proposed, considering the importance of temperature in the ageing of the battery.[34] The CTCV protocol is simple to implement and results in charging that is 20% faster compared with the CCCV protocol.

Chen *et al.* introduced sinusoidal ripple charging (SRC), claiming a reduced charging time, and an improved charging efficiency and battery lifetime with a controlled increase in the temperature of the battery.[35] A challenge in using SRC for practical chargers is precise control over the magnitude and frequency of the charging current. The frequency should be optimal to achieve a low impedance of the battery. Furthermore, the magnitude of the ripple, which affects polarisation in the battery and selection of the components in the charger, needs to be monitored.[36–39] Hence, a new power electronics converter topology for the charger and precise control of the outputs (current and voltage) with the ability to reduce power quality issues for vehicle-to-grid issues has been proposed in ref. 38. Furthermore, the suppression of dendrite growth in the battery is another demonstrated benefit.[40] By contrast, Bessman *et al.* showed that, using experiments on prismatic cells and a physics-based model, the claimed benefits of SRC are not as described in the literature.[41]

In recent years, a new research direction has opened up towards the model-based charging system. Information gathered from the electrical and electrochemical modelling of batteries can be utilised to optimise the charging of the battery. The model-based charging technique uses electrical, electrochemical and thermal models and computes parameters for the battery.[42–49] The parameters computed using the electrical model include the impedance and the SoC.[50–52] The electrochemical model computes the SEI potential or thickness, the active material concentration, and the anode potential. The capacity, temperature and state of health (SoH) are common to the model-based charging techniques. The studies in this research direction have also demonstrated a decrease in the charge time and control of the increase in battery temperature. However, a few reports have considered the effect of battery degradation during charging. Furthermore, the advantage of model-based charging has been demonstrated only partly in simulations because of the requirements of multiple battery parameters that are specific to a particular battery and the need for computational devices with higher memory. The charging service providers prefer to use low-cost, reliable processors to control the charging process of batteries. These low-cost, reliable processors have limited memory and computational capacity.

1.3 Methods

Studying the parameter variations of Li-ion batteries involves experimental procedures that require enormous amounts of time and precision-measurement instruments. Mathematical models that capture various phenomena within the battery can act as a replacement for the experiments. Hence, mathematical models have been proposed widely and used in the literature to design new batteries or manage battery systems. The Butler–Volmer and Nernst equations were the earliest approaches used to describe the physics of batteries. The Butler–Volmer equation relates the current density and the overpotential in batteries.[53] By contrast, the Nernst equation describes the electric potential of the electrode and electrical charge in the battery.[54] These equations are simple, but they are not sufficient to describe the complex physics of advanced Li-ion chemistries. Newman *et al.* developed the porous electrode theory, which became a standard mathematical model for Li-ion batteries. The model has been popularly reported as the

Doyle–Fuller–Newman (DFN) model in the literature.[55,56] The Butler–Volmer and Nernst equations use differential-algebraic equations, whereas the DFN model uses partial differential equations. The equations of the DFN model are solved using a variety of numerical solving tools such as control volumes, finite-difference methods, finite element methods, orthogonal collocation and others. The challenge in using the DFN model is the complexity of solving the equations, even after using the listed variety of numerical solving tools.

Alternatively, equivalent circuits and simplified electrochemical models, such as the single-particle model and the single-particle model with an electrolyte, have been developed to meet the challenges of complexity, computational cost (speed and memory) and fast convergence to obtain results. Although alternative models solve the challenges, reports in the literature reveal that correction factors are required to obtain appropriate results.[57] Hence, the DFN model is selected to analyse the electrical, electrochemical, and mechanical parameters of the battery in this work. The governing equation of the DFN model is classified into three parts: charge conservation, molar conservation and electrochemical reactions. Each part is discussed in detail in ref. 57–59 and in (Section 1.1, ESI†).

1.3.1 Modelling of degradation mechanisms. The degradation mechanisms modelled in the work are for the SEI layer, lithium plating, and particle cracking. The parameters of the battery used for these simulations are given in Table S2 (ESI†).[18] The battery parameters are based on lithium cobalt oxide (LCO) chemistry with graphite as the negative electrode, a polypropylene separator, and $LiCoO_2$ as the positive electrode. Apart from the parameters, various constants used in the simulation are also given in Table S2 (ESI†). The other models aggregated with the DFN model help to analyse the degradation and thermal changes. The model of SEI layer formation is considered from ref. 15, the particle cracking model is considered from ref. 60 and 61, and the thermal model is considered from ref. 58 and 62. A lumped thermal model of the battery is used in which the average temperature of the cell is proportional to the ambient temperature. The equations are given in (Section 1.1.1, ESI†). Furthermore, the thermal model considers the heat exchange between the battery and the environment while simulating the impact of ambient temperature on the rate of battery degradation.

Based on ref. 15, the SEI is considered to be composed of lithium ethylene dicarbonate ($(CH_2OCO_2Li)_2$, or EC). The total transfer current density (j_{tot}) during the intercalation and the side reactions is given by:

$$j_{tot} = j_{int} + j_{SEI} + j_{lpl} \quad (1)$$

where j_{int}, j_{SEI}, and j_{lpl} are the intercalation current density, the SEI formation current density, and the lithium plating current density, respectively. Each current density is defined using eqn (2a), (2b), and (2c). (2a) is based on the Butler–Volmer equation, and eqn (2b), and (2c) are based on the cathodic Tafel equation.

$$j_{int} = ai_{0,int}\left(\exp\left(\frac{\alpha_{a,int}F}{RT}\eta_{int}\right) - \exp\left(-\frac{\alpha_{c,int}F}{RT}\eta_{int}\right)\right) \quad (2a)$$

$$j_{SEI} = -aFk_{0,SEI}c_{EC}^{S}\exp\left(-\frac{\alpha_{c,SEI}F}{RT}\left(\phi_s - \phi_e - \frac{j_{tot}}{a}R_{film} - U_{SEI}\right)\right) \quad (2b)$$

$$j_{lpl} = -ai_{0,lpl}\exp\left(-\frac{\alpha_{c,lpl}F}{RT}\left(\phi_s - \phi_e - \frac{j_{tot}}{a}R_{film}\right)\right) \quad (2c)$$

In eqn (2a), (2b) and (2c), a denotes the specific surface area, η_{int} is the surface overpotential, $i_{0,int}$ is the lithium intercalation exchange current density, $k_{0,SEI}$ is the kinetic rate constant, U_{SEI} is the SEI formation reaction equilibrium potential, c_{EC}^{S} is the concentration of EC on the surface of graphite, and $i_{0,lpl}$ is the Li deposition exchange current density. The parameter η_{int} in eqn (2a) is defined as:

$$\eta_{int} = \phi_s - \phi_e - \frac{j_{tot}}{a}R_{film} - U_{int} \quad (3)$$

where ϕ_s and ϕ_e are the solid phase potential and electrolyte phase potential, respectively, U_{int} is the lithium intercalation reaction equilibrium potential, and R_{film} is the surface film resistance. Furthermore, the EC concentration is computed based on mass conservation as in eqn (4):

$$-D_{EC}\frac{c_{EC}^{S} - c_{EC}^{0}}{\delta_{film}} = -\frac{j_{SEI}}{F} \quad (4)$$

where D_{EC} is the EC diffusivity, c_{EC}^{0} is the EC concentration in the bulk electrolyte, and δ_{film} is the surface film equivalent thickness. The material balance of SEI formation and lithium metal is defined using eqn (5) and (6):

$$\frac{\partial c_{SEI}}{\partial t} = -\frac{j_{SEI}}{2F} - \frac{j_{lpl}}{2F}\beta \quad (5)$$

$$\frac{\partial c_{Li}}{\partial t} = -\frac{j_{lpl}}{F}(1 - \beta) \quad (6)$$

where c_{SEI} and c_{Li} are the SEI and lithium metal molar concentrations per unit volume of the electrode. Since oxidation between lithium metal and the electrolyte is possible when in contact, the parameter β is introduced to define a quantity that denotes the fraction of plated lithium converting to the SEI layer. Furthermore, the SEI layer and the lithium metal together form the surface film that covers graphite particles; here, the amount of SEI and lithium metal used to determine the surface film equivalent thickness is defined as:

$$\delta_{film} = \frac{1}{a}\left(\frac{c_{SEI} \cdot M_{SEI}}{\rho_{SEI}} + \frac{c_{Li} \cdot M_{Li}}{\rho_{Li}}\right) \quad (7)$$

where ρ and M are the density and molar weight, respectively. The surface film resistance is computed using SEI as:

$$R_{film} = \omega_{SEI}\frac{\delta_{film}}{\kappa_{SEI}} \quad (8)$$

where ω_{SEI} is the SEI volume fraction in the film, and κ_{SEI} is its ionic conductivity.

Multiple charging and discharging cycles/schedules lead to stress in the electrode materials, resulting in particle cracking. The particle cracking model in ref. 61 is used in this work. Since it is difficult to measure the particle crack length experimentally, a few assumptions are made to simplify the model. These are (a) the electrode particles have identical microcracks with a length l_{cr}, a width w_{cr} and a crack number per unit area density of ρ_{cr}; and (b) the cracks grow only in length during cycling, and the width and density remain constant. With these two assumptions,[61] the fatigue crack growth model using Paris' law is defined as:

$$\frac{dl_{\text{cr}}}{dN} = \frac{k_{\text{cr}}}{t_0}\left(\sigma_{\text{t}} b_{\text{cr}} \sqrt{\pi l_{\text{cr}}}\right)^{m_{\text{cr}}} \quad \sigma_{\text{t}} > 0, \tag{9}$$

where b_{cr} is the stress intensity factor correction, σ_{t} is the tensile stress, t_0 is the time for completion of one cycle, and k_{cr} and m_{cr} are constants determined using experimental data. Since the crack growth is impacted by only tensile stress in this model, the instantaneous crack area change rate to the volume ratio is estimated using eqn (10):

$$\frac{da_{\text{cr}}}{dt} = \frac{a_{\pm}\rho_{\text{cr}}w_{\text{cr}}}{t_0} \cdot \frac{dl_{\text{cr}}}{dt} = \frac{a_{\pm}\rho_{\text{cr}}w_{\text{cr}}}{t_0} \cdot k_{\text{cr}}\left(\sigma_{\text{t}} b_{\text{cr}} \sqrt{\pi l_{\text{cr}}}\right)^{m_{\text{cr}}} \tag{10}$$
$$\sigma_{\text{t}} > 0.$$

The averaged SEI thickness on the cracks $L_{\text{SEI,cr}}$ with time evolution is defined by:

$$\frac{\partial L_{\text{SEI,cr}}}{\partial t} = \frac{c_{\text{sol,0}}D_{\text{sol}}(T)\bar{V}_{\text{SEI}}}{2L_{\text{SEI,cr}}} + \frac{\partial l_{\text{cr}}}{\partial t}\frac{L_{\text{SEI,cr0}} - L_{\text{SEI,cr}}}{l_{\text{cr}}}. \tag{11}$$

The temperature dependency of the physiochemical properties of the cell is modelled using the Arrhenius equation, defined as:

$$\phi = \phi_{\text{ref}}\exp\left[\frac{E_{\text{act},\phi}}{R}\left(\frac{1}{T_{\text{ref}}} - \frac{1}{T}\right)\right] \tag{12}$$

where ϕ is the diffusion coefficient of the different constituents, T_{ref} is the reference temperature, and $E_{\text{act},\phi}$ is the activation energy of the respective constituent, such as the electrolyte, etc. The details of each model are discussed in the respective articles. The simulation experiments were performed by building, updating and integrating the battery model with the related physics-based thermal and degradation submodels using the Python Battery Mathematical Modelling (PyBaMM) package.[59]

The experimental protocols were developed using PyBaMM to simulate the 15 types of charging technique (as shown in Table 1) at different charging rates and ambient temperatures. The lower and upper cut-off potentials are defined as 2.8 V and 4.2 V, respectively. In the case of pulse charging and pulse charging with discharge, the average current in a cycle is used to define the charging rates. For the CCCV charging protocol, the CC period is used to define the charging rate. Furthermore, once the battery reaches 4.2 V, the CV mode is activated until the current drops to one-tenth of the initial charge rate ($C/10$). The discharging is carried out at a constant rate of 1C for all the experiments. All the simulated experiments were performed for 350 cycles. The results discussed in this article are values of the parameters obtained at

Table 1 Summary of the different types of charging techniques simulated in this work. t_{on}, t_{off} and t_{dis} are the time during a period of pulse to turn on to charge, turn off to rest and discharge, respectively. Each charging technique is simulated using a DFN model with incorporated degradation models at different charging rates. The empty spaces indicate that the specific parameter is not relevant to the charging type

No.	Charging technique	t_{on} (s)	t_{off} (s)	t_{dis} (s)
1	CC			
2	CCCV			
3	Pulse charge without discharge	5	0.2	
4	Pulse charge without discharge	3	0.2	
5	Pulse charge without discharge	1	0.2	
6	Pulse charge without discharge	5	0.1	
7	Pulse charge without discharge	3	0.1	
8	Pulse charge without discharge	1	0.1	
9	Pulse charge with discharge	5	0.2	0.2
10	Pulse charge with discharge	3	0.2	0.2
11	Pulse charge with discharge	1	0.2	0.2
12	Pulse charge with discharge	5	0.1	0.2
13	Pulse charge with discharge	3	0.1	0.2
14	Pulse charge with discharge	1	0.1	0.2
15	Pulse charge with discharge	1	0.1	0.1

the end of each simulation experiment (after 350 cycles). The total lithium concentration in the particles, i.e., positive and negative electrodes, and the total lithium concentration in the electrolytes constitute the overall lithium concentration inside a physical battery. Over the charge–discharge cycles, some of the lithium will be lost to side reactions, viz., lithium plating, SEI growth, and electrolyte reactions with lithium. SEI formation causes a loss of lithium inventory (LLI) by immobilising Li$^+$ ions and impedance changes via film resistance and pore-clogging.[63] Lithium plating causes the LLI in the most literal sense by forming dead lithium, as well as causing some impedance changes via pore clogging.[64] The LLI constitutes the active lithium concentration lost to the aforementioned side reactions. The percentage LLI loss is estimated via two categories, i.e., with and without considering lithium lost to the electrolyte. This can be calculated based on eqn (13) and (14):

$$\text{LLI including electrolyte}\,(\%) = \frac{\text{Total Li lost to side reactions (mol)}}{\text{Initial lithium (mol)}} \\ \times 100 \tag{13}$$

$$\text{LLI}\,(\%) = \frac{\text{Total lithium lost to plating and SEI layer (mol)}}{\text{Initial lithium in particles (mol)}} \\ \times 100 \tag{14}$$

The experiments performed by simulating different charging techniques are focused on meeting the objective of proposing a battery-friendly charging technique irrespective of the change in ambient temperature and the requirements of any C_{rate}. The results obtained are analysed to find the impact of the change in C_{rate}, charging technique, ambient temperature and changes in the properties of the charging pulses. The properties of the charging pulses under consideration are increase or decrease in the time period of pulses (T), t_{on}, t_{off}, the amplitude of charge and discharge pulses invariants of pulse charging.

The extensive simulations and analysis performed on the selected battery help to propose a charging technique that is suitable for either energy-extensive or power-intensive applications.

1.4 Parameters studied in the literature to propose new charging technique

The parameters of Li-ion batteries studied in the literature are either electrical, electrochemical, or mechanical in nature. The electrical parameters studied are the impedance, SoC, SoH, capacity (fade, retention, relative, incremental, and utilisation), energy efficiency, variations in the OCV voltage, and the specific energy. The electrochemical parameters include the rate of side reactions, the overpotential, the active material volume concentration in the electrodes, the SEI (thickness, density, film resistance, and potential), lithium loss, side reaction exchange current density, electrode potentials, and the polarisation voltage. The porosity, electrode particle cracking, structural disordering, stress and expansion of the cell (width and length) are the mechanical parameters studied in the literature. The temperature rise, the change in charging time, and the rate of capacity fade result from a variation in these parameters.

The CCCV is the standard, and oldest, technique described in the literature. Hence, all the new proposed charging algorithms compare variation of the parameters listed above with the CC–CV method. Moreover, impedance was the most commonly studied parameter in earlier studies because of the possibility to relate it with variation of the SoC, as well as battery degradation.[14,23,24,65,66] Table 2 list the types of parameter studied for the different types of charging technique. The maximum number parameters is studied in the CC–CV charging technique, which is the oldest and standard. By contrast, the least number of parameters are studied in the temperature-based charging technique.[34]

Studying the variation in the types of parameter for each charging technique is associated with the rate of battery degradation. Although the literature has described multiple studies on each charging technique, to prove the suitability of rapid charging and reduced battery degradation, there is a lack of studies that associate all three types of parameter (electrical, chemical, and mechanical). Furthermore, only a few studies describe the effect on the parameters due to an increase or decrease in the ambient temperature. Hence, the commercially used charging techniques (i.e., CC, CCCV, pulse charging (with a negative pulse and without a negative pulse) and variable frequency/duty charge pulse) will be analysed in detail to understand and associate the change in the three types of parameter with the degradation phenomenon.

In this work, the overpotential, the extent of lithiation in the electrodes, the inactive material volume fraction and the SEI layer thickness in the electrodes, the loss of capacity due to lithium plating, and the loss of lithium are studied as the chemical parameters. The porosity, tortuosity, and the phenomenon of particle cracking in the electrodes are included as mechanical parameters, while the resultant parameters such as the energy, power, and capacity fade are analysed as electrical properties. Li-ion batteries undergo two reactions during charging and discharging, i.e., primary intercalation and secondary electrochemical reactions (also called side reactions). The intercalation reactions are responsible for the charge and discharge of batteries. By contrast, the side reactions lead to the loss of lithium and materials, which intervene in intercalation reactions called active materials. Side reactions also lead to electrolyte oxidation and reduction, passivation, structural disordering, particle cracking, thickening of the SEI layer and lithium plating. The results of side reactions lead to capacity fade in the battery, which will be described in the subsequent subsections. The SEI layer thickness, particle cracking, and a change in the internal cell temperature are the major parameters that impact the discharge capacity of batteries.[10,12,13] Hence, they are included in the main study, while others are described in ESI† section. Furthermore, the temperature (especially low temperature) and C_{rate} (higher) together impact the loss in capacity due to lithium plating.[67] Hence, they are discussed in the subsections where the impact of the change in ambient temperature is also included (Table 3).

Table 2 Different types of parameter studied or used in models reported so far. The electrical model requires the least number of parameters to be modelled but helps to derive the required health status. The electrochemical model is computationally expensive and demands numerous parameters, which are either available only to the manufacturer or determined using sophisticated tests and equipment. The mechanical model is also similar to the electrochemical model, but the governing equations used are different. Both the electrochemical and mechanical models help in determining the health of the battery

Charging technique	Electrical	Electrochemical	Mechanical
CCCV	Capacity, impedance, efficiency (charge and energy), OCV, SoC, and SoH	Electrode potential, side reaction rate, active material concentration, lithium loss, SEI (thickness, density, and resistance), and exchange current density.	Porosity, stress, expansion (cell width and length), structural disordering
Pulse charging	Capacity, impedance, SoC, and efficiency (charge and energy)	Li-loss, surface concentration, and transfer reaction	Structuring disordering and porosity
Model-based	Impedance, differential voltage, SoC, SoH, ohmic loss, capacity, and energy	Polarization voltage, SEI (thickness and potential), electrode potential, Li concentration, and active material concentration	
Boost charging	Capacity, and charge efficiency	Concentration (electrolyte, surface) transfer reaction	Porosity
Temperature-based	SoC, impedance, capacity, SoH and end-of-life		

Table 3 Summary of the variation in parameters with an increase in the charging rate for the different charging techniques

		CC	CCCV	Pulse charging without discharge				Pulse charging with discharge				
									Amplitude of discharge current			
No.	Parameter	C_{rate}#	C_{rate}#	t_{on}†	t_{off}†	t_{on} and t_{off}†	C_{rate}#	t_{on}†	0.5	1	2	C_{rate}#
1	X-averaged negative electrode inactive material volume fraction (Fig. S1, ESI)	⇓	⇓	⇓	⇓	⇓	⇓	⇓	⇓	⇓	⇓	⇓
2	X-averaged total negative electrode SEI thickness (nm) (Fig. 3a)	⇓	⇓	⇓	⇓	⇓	⇓	⇓	⇓	⇓	⇓	⇓
3	X-averaged negative electrode porosity (Fig. S4, ESI)	⇓	⇓	⇓	⇓	⇓	⇓	⇓	⇓	⇓	⇓	⇓
4	X-averaged negative electrode tortuosity (Fig. S5, ESI)	⇑	⇑	⇑	⇑	⇑	⇑	⇑	⇑	⇑	⇑	⇑
5	X-averaged negative electrode reaction overpotential (V) (Fig. S2, ESI)	⇑	⇑	⇓	⇓	⇓	⇑	⇓	⇑	⇓	⇑	⇑
6	X-averaged negative electrode extent of lithiation (Fig. S3, ESI)	⇓	⇓	⇓	⇓*	⇓	⇓	⇓	⇓	⇑	⇑	⇓
7	X-averaged cell temperature (K) (Fig. 3c)	⇑	⇑	⇑	*	⇓	⇑	Low C_{rate} = ⇑ and high C_{rate} = ⇓	⇓	Low C_{rate} = ⇑ and high C_{rate} = ⇓	⇓	⇑
8	Capacity fade (Fig. 3d)	⇑	⇑	⇓	⇓*	⇓	⇑	⇑	⇓	⇑	⇑	⇑
9	X-averaged negative electrode particle crack length (Fig. 3b)	⇑	⇑	⇑	⇑	⇑	⇑	⇑	⇓	⇑	⇑	⇑

†, #, ⇓, ⇑, and * denote decreasing, increasing, a decreasing trend, an increasing trend and a negligible change, respectively.

2 Results

2.1 SEI layer thickness

Side reactions in Li-ion batteries occur in three major regions: at electrode–electrolyte interfaces, at electrode–collector interfaces, and in the electrolyte.[68] A change in the equilibrium potential of the reactions during charging and discharging leads to instability in the electrolyte. This instability is accompanied by the start of side reactions within the battery.[69] The change in the equilibrium potential depends on the amplitude of the charging current and the types of charging. Hence, the concentration of the inactive materials and the electrode–electrolyte interface or SEI layer thickness varies for different charging types and rates. Despite being a by-product of side reactions, the SEI layer serves as a protective layer in graphite particles of negative electrodes in the battery. The lithium potential makes the electrolyte unstable and vulnerable to the reaction, which leads to the loss of lithium and a reduction in the overall capacity of the battery. Since it is a form of inactive material, the variation in the concentration of inactive material and the thickness of the SEI layer are similar, as shown in Fig. S1 (ESI†) and Fig. 3a. A comprehensive discussion on the formation of inactive material for different types of charging is discussed in the (Section 1.2, ESI†). The thickest SEI layer is formed in CC and CCCV, followed by CT9, which is pulse charging with discharge. The SEI layer thickness for all charging rates is also the highest in CCCV. During CCCV, the time for the CV phase is higher and increases with an increase in the number of cycles. During CV, the stress due to electrochemical reactions and temperature is lower than the CC phase, leading to the formation of a stable SEI.[8] Hence, with an increase in the number of cycles, the SEI layer keeps becoming thicker. Furthermore, the formation of the SEI is also higher at lower charging rates, for the same reason as seen in Fig. 3a.[20]

The plot in Fig. 3a shows that pulse charging has the potential to reduce the SEI layer thickness. The SEI layer thickness in charging types 3–8 (CT3–CT8), which is pulse charge without discharge, varies with the change in t_{on}. The thickness is highest for CT3, which has the highest t_{on}, while CT8 is the lowest because of the lowest t_{on}. The t_{off}, too, impacts the thickness of the SEI layer. The SEI layer thickness is reduced with a decrease in the t_{off}. A reduced t_{on}, as well as a reduced t_{off}, helps to suppress the thickness of the SEI layer. A larger t_{on} at a lower C_{rate} acts similarly to the CCCV method. Even at a higher C_{rate}, the pulse rest phase will help to stabilise the SEI layer, leading to thickening with an increase in the number of cycles. Hence, decreasing t_{on} and t_{off} helps to reduce the thickening of SEI layers.

The variation in the change of SEI layer thickness for pulse charging with discharge is shown in CT9–CT15 in Fig. 3a. Most of these pulse charging with discharge examples help to reduce the SEI layer thickness. The SEI layer thickness has a reducing trend for CT9–CT11, although the variation is not much for CT10 and CT11. The amplitude of the discharge current, too, has a role in the change in the SEI layer thickness. When the amplitude of the discharge current is equal to the average current (CT9–CT11), with the reduction in t_{on}, the SEI layer thickness is also reduced.

Furthermore, when the amplitude of the discharge current is equal to half of the average current (CT12 and CT13), a higher on-time results in a lower SEI layer thickness. By contrast, when the amplitude of the discharge current is equal to the twice the average current, a higher on-time results in a thicker SEI layer. The change in the polarity of the charge pulses leads to a similar variation of the equilibrium potential. When the amplitude of the current in the discharge pulse is more than the charge pulse, the equilibrium potential falls below the stability limits of the electrolyte, accelerating the SEI formation. The rest
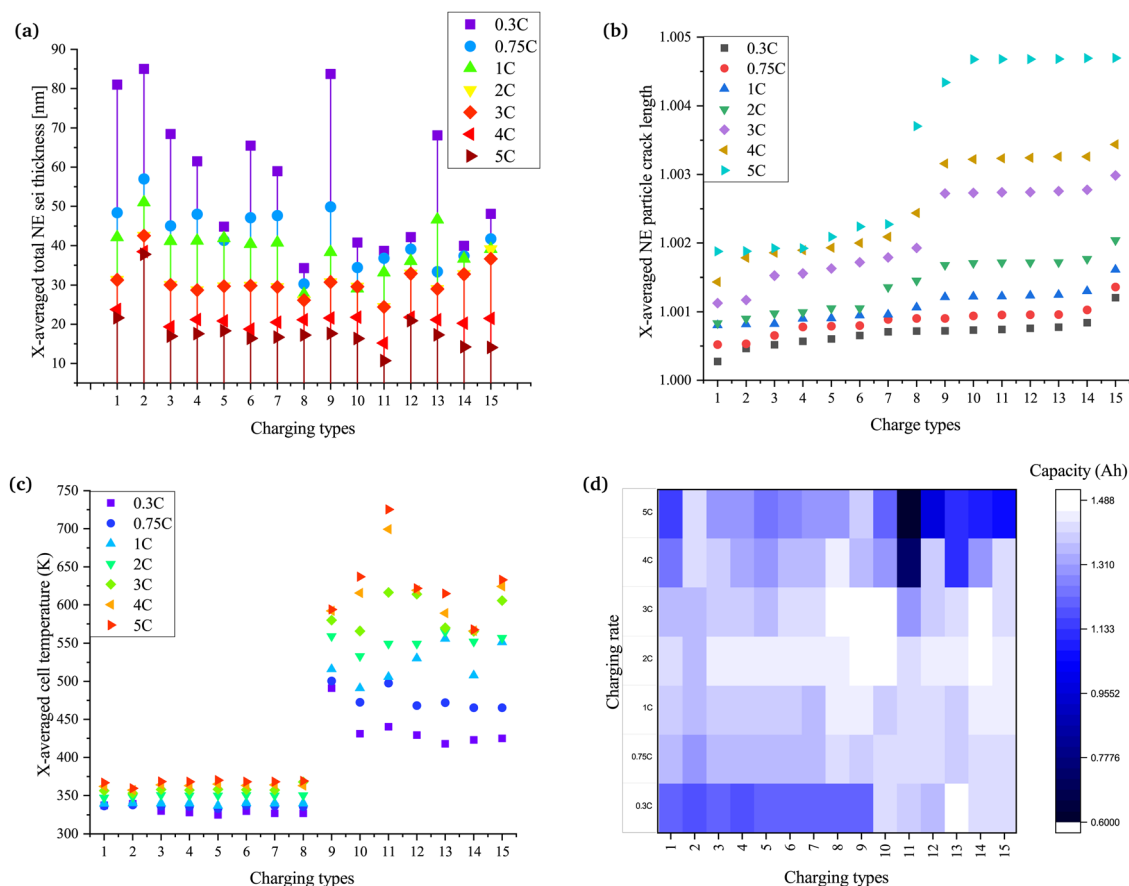
Fig. 3 Variation of the parameters of the batteries for different charging techniques and charging rates at the end of 350 cycles: (a) the X-averaged total negative electrode SEI thickness (nm) decreases with an increase in C_{rate} as the chemical degradation is dominant at slower C_{rate}; (b) the X-averaged negative electrode particle crack length increases with an increase in C_{rate} because of the increased stress in the electrode particles; (c) the X-averaged cell temperature (K) is higher for higher C_{rate} due to the increase in chemical kinetics, where the discharge pulses further instigate the phenomenon because of the change in the direction of motion of ions and masses; and (d) the capacity fade varies for different charging techniques and rates, and is also a function of the chemical and mechanical parameters and internal changes in temperature, which are impacted by the charging technique and rate.

phase further helps to stabilise the SEI formed, leading to a thick SEI layer in comparison with when the amplitude of the current in the discharge pulse is less than or equal to the charge pulse. The charge type with the amplitude of the discharge current equal to the average current and the least t_{on} and rest time show the thinnest SEI layer formed over the negative electrode.

2.2 Particle crack length

Particle cracking is a form of mechanical degradation in batteries that is observed in the electrode particles. The stress in the electrode particles is commonly modelled or reported experimentally due to intercalation/deintercalation reactions and changes in the internal cell temperature or ambient temperature. The crack in the particles results in the exposure of active materials to the surface, leading to side reactions. These side reactions then lead to heat generation, amplifying the phenomena of stress and side reactions due to an increase in the cell kinetics.[70] Hence, an increase in mechanical degradation increases chemical degradation and *vice versa*.

Fig. 3b shows the variation of the particle crack length on applying the different charging techniques at different charging rates. The slower charging rates resulted in the least amount of particle cracking. There is an increase in the particle crack length going from left to right. The CC and CCCV methods (CT1 and CT2, respectively) resulted in the lowest crack length, although CCCV has higher values compared with CC. This is because, at a higher battery potential, the stress on the particles of the electrodes is higher, and CCCV results in a higher crack length. In the CC method, the battery is allowed to settle with a reducing charge current. Since the battery is not allowed to settle and the overpotential remains higher (Fig. S2, ESI†), the stress due to the increased potential of the battery and saturation of the electrodes is not experienced. The overpotential is difference between the thermodynamic or equilibrium potential and the potential at which the redox event can be experimentally observed. A detailed discussion on the variation of the overpotential with the change in the charging types is presented in the supplementary text (Section 1.3, ESI†). However, in the case of the CCCV method, the battery keeps charging after switching to CV. With the increase in potential, the stress on the particles of the

electrodes continues to increase, and hence the particle crack length is greater than in the CC method.

The pulse charging techniques that resulted in a better candidate for rapid charging when previous parameters were considered do not perform well. The reason behind the increase in the crack is related to the heat generated during the intercalation and deintercalation reactions. The heat generation adds to the internal battery temperature rise and increases the chemical kinetics and the stress in the electrode particles. The higher the increase in the internal cell temperature (Fig. 3c), the higher the particle crack length. Hence, a change in the ambient temperature may result in an increase or a decrease in particle cracking. During pulse charging with discharge (CT9–CT15), the increase in the amplitude of the discharge pulse resulted in a further increase in the particle crack length.

2.3 Cell temperature

The internal cell temperature is a significant factor that impacts the capacity fade of batteries. The temperature brings about changes in the equilibrium potential of reactions within the battery, the chemical kinetics that affect the rate of side reactions, the formation and erosion of the SEI layer, the diffusivity of charge and mass in the electrodes, stress in the battery, structure disordering of the electrodes and overall geometry, and safety during operation of the battery.[71,72]

A higher C_{rate} results in an increase in the heat generation due to the rapid diffusivity of charges and increased stress in the electrode particles. The conventional CC and CCCV methods have control over the rise in the internal cell temperature. However, the temperature rose to a very high value during pulse charging with discharge (CT9–CT15). The temperature rise is related to the ease of the diffusivity of charge in the battery during both intercalation and intercalation. With an increase in the SEI layer thickness, a decrease in porosity and lithiation, and an increase in the tortuosity of the electrodes, a resistance to charge and mass transfer is offered (Fig. 3a and Fig. S3–S5, ESI†). Lithiation, porosity and tortuosity impact the diffusion of ions with the electrodes, hence impacting the resistance of the cells. A detailed discussion on the lithiation, porosity and tortuosity is presented in the (Sections 1.4, 1.5 and 1.6, ESI†). The increase in the resistance adds to heat generation and impacts the electrolyte stability.

The impact of the increase in internal cell temperature is deteriorating by nature. The increase in the temperature induces stress in the electrode particles and erodes the SEI layer. On erosion, the surface of the active material or electrode particles is unlatched to undergo further side reactions. Apart from forming the SEI layer, the side reactions leave behind residual inactive materials and gases are generated due to the phase transition from solid to gas or liquid to gas. An uncontrolled rise in the temperature will lead to thermal runaway and harm the safety of the battery when being charged or discharged. Fig. 3c indicates that conventional CC and CCCV (CT1 and CT2) and pulse charging without discharge (CT3–CT8) are effective methods to perform rapid charging with a limited rise in the internal battery temperature.

2.4 Discharge capacity

The discharge capacity is the final parameter of the battery, which determines its performance. The discharge capacity depends on the various parameters discussed in previous subsections. A reduction in capacity fade depends on the C_{rate} and the charging techniques used, as shown in Fig. 3d. The C_{rate} impacts the rate of chemical kinetics, the equilibrium potential and stress due to intercalation reactions. An increase in the mentioned parameters increases the overpotential, whereas a decrease in the mentioned parameters reduces the overpotential. At higher C_{rates}, the overpotential rises and increases the terminal voltage. Since the battery terminal voltage reaches the cut-off potential much earlier, the electrode is not lithiated completely. The battery does not charge to the full range of SoC. When the CCCV method is used for charging, the CV part of charging allows the battery to be charged on a broader SoC range as the rise in overpotential is countered by the fall in current. Furthermore, the charging time and rates also impact the reduction in discharge capacity. A longer charging time at a higher at higher C_{rate} will lead to increased stress on the electrode particles due to increased concentration gradients.[20] This increased stress adds to SEI erosion and more side reactions, leading to a loss of active particles and Li-ions.[73]

In Fig. 3d, it can be seen that the CCCV method (CT2) leads to a larger capacity loss at a slower C_{rate} compared with the CC method (CT1), but at a higher C_{rate}, the CC method leads to larger capacity loss. A similar pattern is also seen in the case of pulse charging without discharge (CT3–CT8). The t_{on} and t_{off} times also impact the reduction in discharge capacity. A decrease in t_{on} and t_{off} is instrumental in countering the reduction in discharge capacity. Considering this, it is observed that higher charging rates are a possible solution with pulse charging without discharge, although 2C is found to be the optimal C_{rate}.

Looking into the pulse charging with discharge (CT9–CT15), an increased t_{on} leads to a similar pattern of reduction in the discharge capacity. The reduction in t_{on} helps to reduce the rate of reduction of the discharge capacity. The discharge pulse amplitude during charging also impacts the discharge capacity change. When the amplitude of the discharge pulse is greater than or equal to the average charging current, the discharge capacity is reduced drastically. This drastic reduction can be related to the change in the equilibrium potential of the reactions and the overpotential during the charge, rest and discharge durations. The rise in internal cell temperature due to increased cell kinetics cannot be neglected when selecting an optimal fast-charge technique. The pulse charging with discharge techniques increase the internal cell temperature to a higher value, leading to thermal runaway. Considering the reduction in the discharge capacity, CT5 is the best technique to charge the battery at a higher C_{rate}.

2.5 Comparison of the results with the change in ambient temperature

Various studies in the literature have reported the impact of ambient temperature on the operation and ageing mechanisms

of the battery at different C_{rate} values. However, the effect of the charging type has not been a widely discussed topic in the literature, although a few studies have suggested charging techniques for extreme temperature conditions.[32] Hence, this work is further extended to analyse the impact of the charging technique at two extreme temperatures, *i.e.*, 318.15 K (45 °C) and 273.50 K (0 °C). The temperature changes the rate of formation of inactive materials, including the SEI, erosion or decomposition of the SEI and instability in electrolytes, resulting in reduction reactions with the active material. The rise in internal temperature above a certain level (125–180 °C) can lead to thermal runaway, venting, and complete destruction of the battery.[74]

The previous results, which were at 298.15 K (25 °C), are compared with the results obtained at two extreme temperatures for four selected charging techniques. CT5 and CT8, which are variants of pulse charging, resulted in the best-performing charging types based on previous simulations at normal ambient temperature. Hence, further simulations were performed only on four charging techniques to reduce the simulation time, *viz.*, CC and CCCV (conventional methods), and CT5 and CT8, which are simulated only at two extreme temperatures.

Fig. 4 and Fig. S7 (ESI†) show all the parameters studied to determine the battery's performance at different charging rates and temperatures. Three different temperatures are represented by "L" (273.50 K (0 °C)), "N" (298.15 K (25 °C)) and "H" (318.15 K (45 °C)). The parameters analysed are those presented in Fig. 3 with added plots for the loss of capacity (Fig. 4b) and the percentage loss of lithium inventory to lithium plating (Fig. 4c). The difference in the formation of inactive material for the different C_{rate} values is the lowest in the case of CT5 (Fig. S7a (ESI†)). For CC, at a lower C_{rate}, the variation in the formation of inactive material is negligible with a change in the temperature. The change in overpotential of the battery is also low; thereby, the changes in the SEI layer thickness, porosity, and tortuosity also follow a similar pattern. The parameters that shows differences are the lithiation, particle crack length and capacity. The changes in lithiation are related to the rate of diffusivity, which changes with the change in the temperature. At lower temperatures, the higher resistance to the diffusion of ions is found in the batteries, resulting in decreased lithiation. With an increase in the temperature, the Li-ions and mass transfer rate increase with an increase in the chemical kinetics. As the lithiation increases, there is an increase in the stress in the particles of the electrode. Hence, as expected, particle cracking increases with the temperature. In general, the loss of lithium inventory reflects chemical degradation. The results align with the findings stated in ref. 20 and 21, where the lower charging rate leads to a higher loss of lithium inventory. The variation in the percentage of lithium loss is found to be the least in the case of CT5 and CCCV.

The temperature changes do not result in a major change in the parameter when the CCCV method is used. However, there is a rise in the formation of inactive materials, the SEI layer thickness, the overpotential, lithiation, tortuosity, and a reduction in the percentage of lithium inventory. Porosity decreases while the particle crack length does not differ

significantly with the CC method. Lithium plating, which is a type of degradation leading to a loss of lithium inventory, is an important phenomenon to be considered when studies at a higher C_{rate} and low temperature are performed.[67] The capacity loss due to lithium plating is found to dominate at lower temperatures and at a higher C_{rate}. A closer look into Fig. 4b shows that CT5 is able to restrain the loss of capacity due to lithium plating, although the losses are higher at extremely fast charging rates.

CT5, which is found to be the best charging technique, shows the lowest variation in values of the parameters at different charging rates. A decrease in t_{on} and t_{off} results in changes as described in previous subsections. The results with reduced t_{on} and t_{off} align with the findings in ref. 75, where it is shown that low-frequency diffusion leads to a higher impedance of the battery. The impedance of the battery is due to an increase in the growth of the SEI layer and the formation of inactive materials. CT8, which follows CT5 in performance, shows a similar pattern of results to that found in the CC, CCCV and CT5 methods.

2.6 Suitability of the type of charging for high-power or high-energy applications

The degradation of Li-ion batteries in EVs also depends on the application. EVs in the transport sector range from small two-wheeled vehicles to large buses. The fast EV racing cars could also not be neglected. The variation in the torque and speed requirements of EV motors changes the discharge pattern of batteries. Hence, the degradation rate also varies for the same battery used in different applications. In this work, an analysis to determine the performance of batteries for higher-energy or higher-power applications is also carried out. Fig. 5 shows plots of terminal power *vs.* energy for the different charging techniques and C_{rate} values.

Fig. 5a shows the plot for the lower ambient temperature. CT5 shows the best performance up to $2C_{rate}$ for all the temperature conditions under study. The CCCV method becomes a competitor under normal temperature conditions, although it is still outpaced by CT5. Furthermore, CCCV shows the worst performance in the low and high ambient temperature regions. These results clearly show the requirements of different charging patterns for different types of vehicles. Fig. 5b shows the plot for the normal ambient temperature range. Here, CT5 and CCCV are close competitors, while CT8 and CC are far behind and are not suitable for use. From Fig. 5c, which shows the plot for the higher ambient temperature range, CT5 is shown to be the best charging technique. The higher charging rate still remains a challenge for all ambient temperature conditions. The solution to the problem is discussed in the next section.

3 Discussion

The benefits of Li-ion batteries and their wide application in EVs have driven research interests for meeting the challenges.
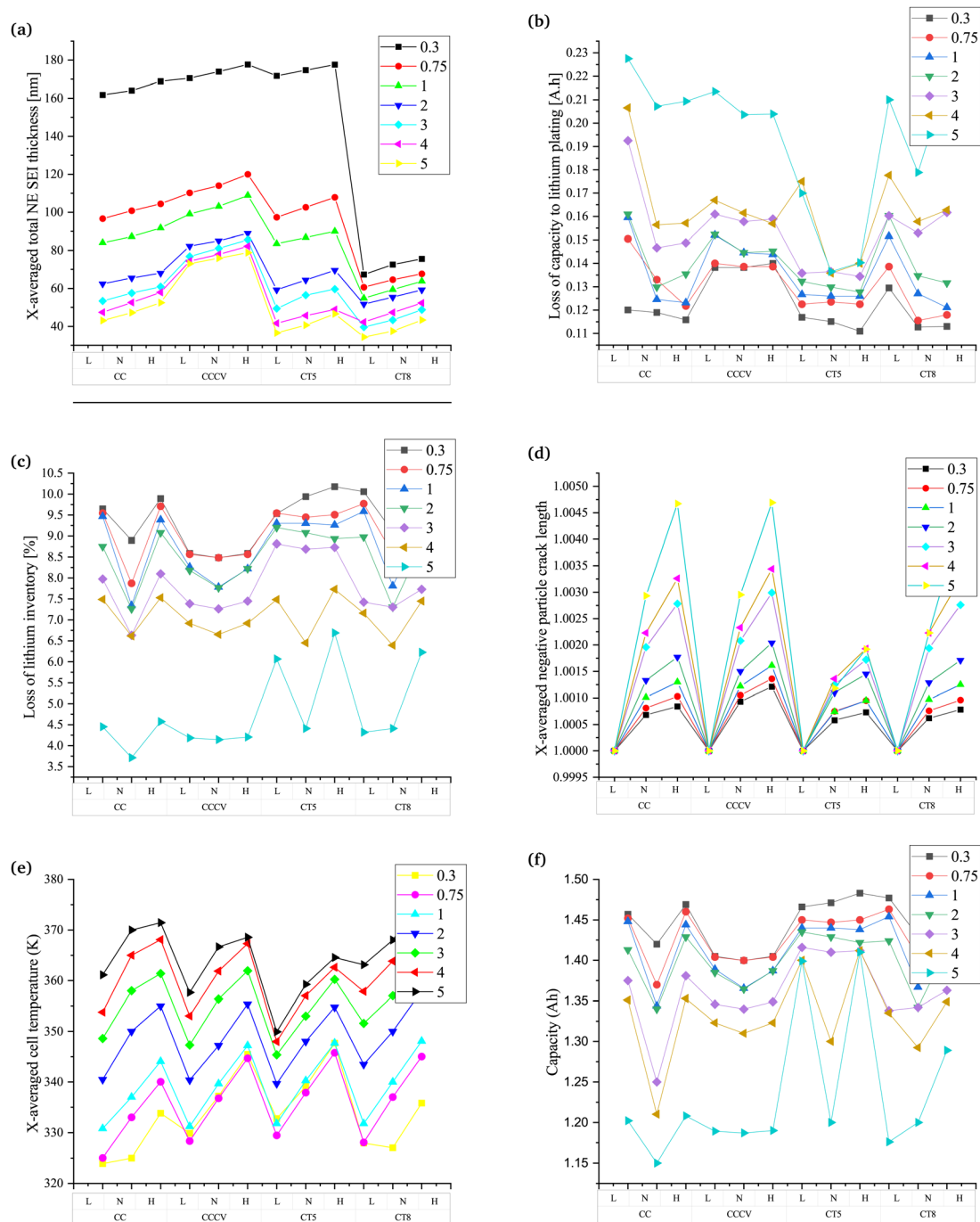
Fig. 4 Variation of different parameters of the batteries at the end of 350 cycles: (a) an appropriate value of t_{on} and t_{off} help in reducing the X-averaged negative electrode SEI thickness (nm); (b) the variation of capacity fade is the highest at a lower temperature and a higher C_{rate}, where CT5 is found to be helpful in constraining the rate of capacity fade due to lithium plating; (c) the percentage loss of lithium inventory is the highest at a lower C_{rate} and reduces with the increase in C_{rate}, where the temperature also impacts the percentage reduction; (d) the X-averaged negative electrode particle crack length is also minimised when CT5 is used; (e) variation of the X-averaged cell temperature (K) of the cell with changes in the ambient temperature, charging rates and charging techniques; and (f) the variation in capacity fade is the highest at a higher C_{rate}, and CT5 is found to be helpful in constraining the rate of capacity fade.

All of the challenges in EVs converge to one aspect: battery degradation.[4,8] The rate of battery degradation changes according to how the EV battery is used, and depends on the EV driver's behaviour, the temperature of the environment, and the EV utilisation type (in high-energy or high-power applications). Higher energy and power density requirements result in a series-parallel connection of cells, which adds to the challenges of making the pack safe, durable, and lower cost. Battery

degradation is triggered by a change in the equilibrium potential of the reactions in the battery. The thermodynamic force to drive the reactions in the battery is associated with the equilibrium potential. Hence, changes in the internal battery or external ambient temperature lead to various chemical and structural alternations.[76]

An increase in the temperature leads to heightened kinetics for both intercalation–deintercalation and side reactions. Compared with normal temperatures, the inactive material formed at elevated temperatures has a different morphology. Most importantly, the SEI layer composition changes. Studies have been performed using differential scanning calorimetry and accelerated rate calorimetry to determine the cell or electrode behaviour.[77,78] These studies explained the phenomenon of self-heating due to exothermic side reactions. Selection of the electrolyte salt has a significant role in the temperature rise. The elevated temperature further erodes the existing SEI layer over the active material. The eroded SEI is either dissolved or re-precipitated, leading to reformation *via* increased side reactions. A more stable SEI and inorganic products are formed, such as lithium fluoride and lithium carbonate.[79] Furthermore, these stable products are less penetrable for Li-ions, thereby the decreasing SEI's overall diffusivity and ionic conductivity.

At low temperatures, degradation of the battery occurs due predominantly to lithium plating, and dendrite formation and a change in the SEI formation do not play a major role.[13,80] Literature reports state that, at low temperatures, the equilibrium potential of the intercalation reactions drops close to the lithium metal potential.[81] Furthermore, viscosity changes in the electrolytes are observed, leading to a decrease in the diffusivity of Li-ions into the electrolyte and electrodes. Li-metal reactions in the electrolyte lead to side reactions, which accelerate the ageing process and increase the capacity loss. The saturation of electrodes due to slow diffusion and the settlement of Li around the electrodes add to the increase in local potential. Hence, the possibility of Li metal plating or dendrite formation increases.[67]

The discussions in this subsection help gain insights into the different types of charging technique discussed in this work. The conventional techniques, *viz.*, CC and CCCV, have shown increased chemical degradation during a lower C_{rate} and increased mechanical degradation during a higher C_{rate}. The overall chemical degradation analysed considering the percentage loss of lithium at different C_{rate} values and at ambient temperature are less on comparing the conventional CC and CCCV methods during pulse charging without discharge, as shown in Fig. 4c. Furthermore, the loss of capacity due to lithium plating, the formation of inactive materials and the SEI layer formed at all C_{rate} values is higher in conventional charging techniques when compared with pulse charging without discharge, as seen in Fig. 4b and Fig. S7a (ESI†), Fig. 4a and Fig. S7 (ESI†) presents the plots for variation of the other parameters not included in Fig. 4. These parameters are the inactive material volume fraction, the electrode reaction overpotential, lithiation, porosity, tortuosity, and the cell temperature. Similarly, the particle cracking length is also higher. The CT5 method shows the best results in terms of all the parameters analysed in Fig. 4, even when the ambient temperature is taken into consideration and the performance does not deteriorate. Hence, the pulse charging technique without a discharge pulse and with a reduced t_{on} and t_{on} can be a suitable option for rapid charging and constraining the battery degradation. The values of t_{on} and t_{off} are an optimization problem given in ref. 82.

Although the CT5 results are optimal for all temperature conditions analysed in this work, the design of new charging techniques will be indispensable at extreme temperatures, such as −20 °C and 80 °C. Furthermore, each charging technique has advantages and disadvantages that can be utilised for charging under extreme environmental conditions. The amalgamation of the charging techniques directs us towards developing a new rule-based charging strategy for Li-ion batteries. Furthermore, for high-energy and high-power applications, the rules can be framed by selecting the suitability of the charging type from Fig. 5, monitoring the rise in the internal battery temperature and appropriately varying the C_{rate}.

The rule-based charging strategy should incorporate the battery electrochemistry, the present battery health parameters, the environmental conditions, user requirements and grid conditions. Hence, this work proposes a new rule-based charging strategy for rapid charging with reduced battery degradation. Different types of electrochemistry for Li-ion batteries are commercially available, *e.g.*, lithium cobalt oxide (LCO), lithium manganese oxide (LMO), lithium iron phosphate
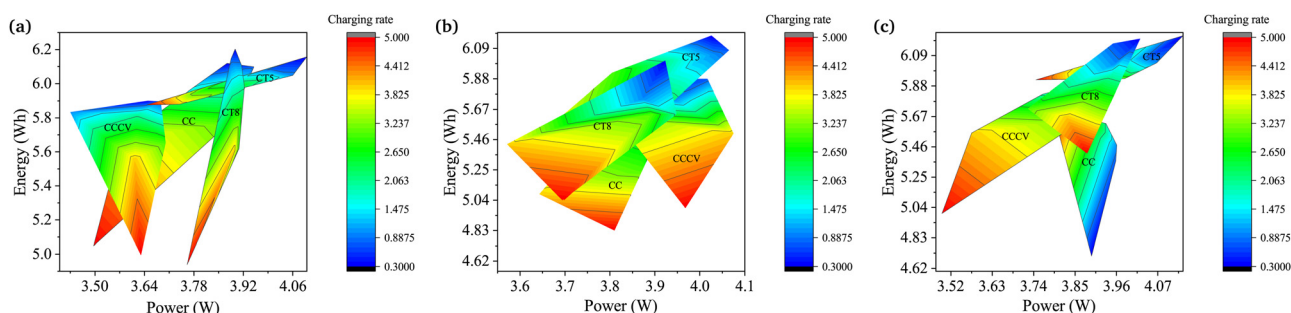

Fig. 5 Variation of the terminal power and energy of the battery for different charging techniques and charging rates at different temperatures: (a) at very low ambient temperature (0 °C); (b) at normal ambient temperature (25 °C); and (c) at high ambient temperature (45 °C).

(LFP), and lithium titanate (LTO). The battery electrochemistry is to be considered because of the variation in the ability to charge rapidly, the performance, lifespan, specific power, and energy. The present battery health conditions will help to determine the ageing of the battery. Capacity estimated by the battery management system (BMS) or any type of model or the previous battery charge and discharge profile data will help to determine the battery's ageing. The environmental conditions include the temperature of the region. User requirements can be a rapid, medium or slow charge. The grid conditions should also be incorporated to avoid the impact of uncoordinated charging, which leads to voltage imbalance and instability.[83–86] The electric grid can be at peak, off-peak, or under normal conditions.

Assuming that an EV arrives at a charging station with the LTO battery electrochemistry. The battery is new and can charge to full capacity, as communicated by the BMS. The temperature of the region of the charging station is below

normal (*i.e.*, −10 °C). The user opts for a rapid charge, and the grid is at peak load condition. For the given scenario, the grid will be overburdened if a rapid charge is performed. Hence, the user will be given the option to go with a slow or medium charge rate. If the user wants to continue with the rapid charge, the service will not be denied, and rapid charging will be selected. The only condition to be evaluated is the ambient temperature. Since the temperature is very low, the battery is under stress, the internal resistance is high, and the possibility of lithium plating is also high. The rise of the internal resistance is due to the low ionic and mass diffusivity. Suppose that the battery's internal temperature is increased, and the viscosity of the electrolyte and the overall rate of diffusion can be brought to normal. The analysis in the previous subsection has shown that pulse charging with discharge can help to increase the battery's internal temperature. Hence, the battery undergoes a pulse charging with discharge for a period of time until the battery's internal temperature
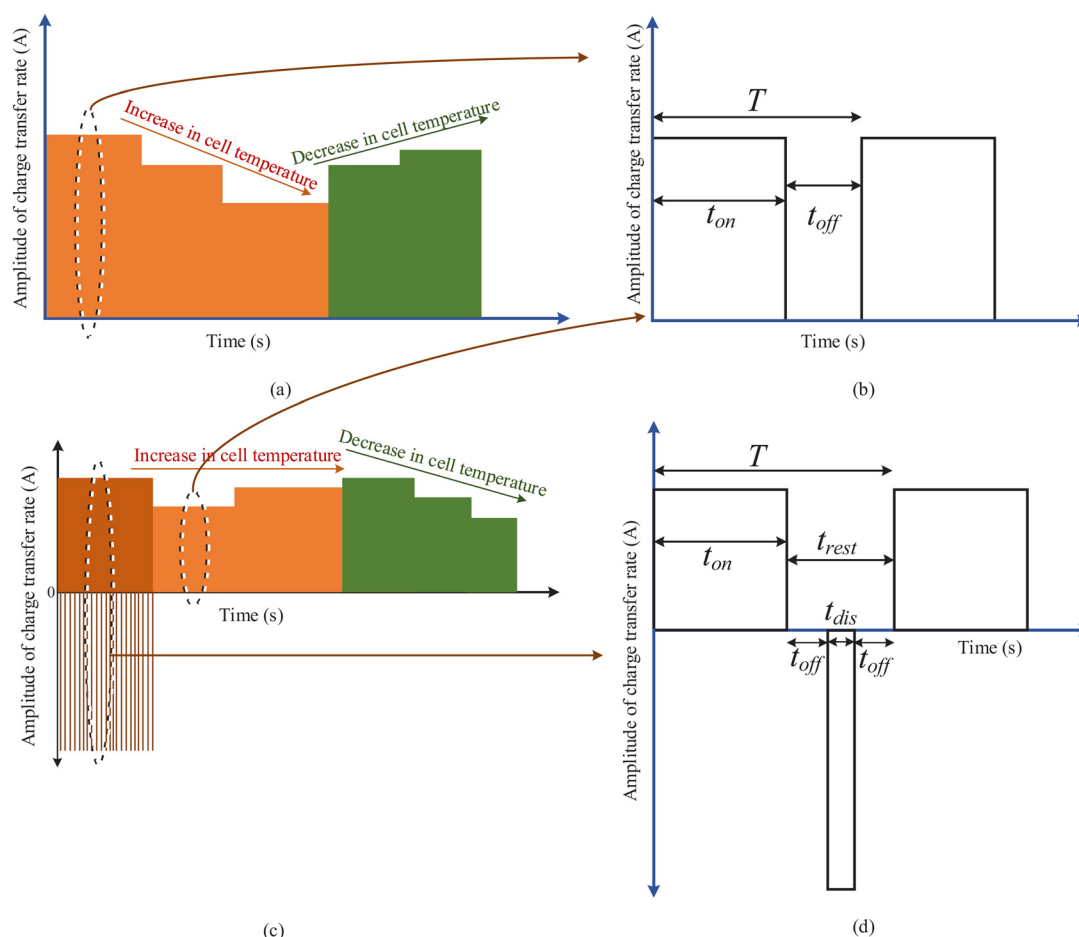
Fig. 6 Proposed charging technique. (a) The charging pattern that is suitable for charging at normal or high ambient temperatures. The increase and decrease in the cell temperature are countered by reducing and increasing the amplitude of the positive pulse current. (b) Pulse charging without discharge pulse: the pattern of the pulse in which T, t_{on} and t_{off} are required to be computed to constrain battery degradation. (c) The charging pattern that is suitable for charging at extremely low temperatures. (d) Pulse charging with a discharge pulse: the pattern of the pulse in which T, t_{on}, t_{off}, and t_{dis} need to be computed to constrain battery degradation. The discharge pulse of more than the average charging current helps to increase the internal cell temperature. The increase and decrease in the cell temperature, in this case, are controlled by shifting from pulse charging with discharge to pulse charging without discharge and increasing or decreasing the amplitude of the charge current.

becomes normal. Later, with controlled battery temperature monitoring, rapid charging can be performed using a charging pattern, leading to the least battery degradation. For instance, in this work, CT8 is found to be the best performer. Similarly, for LTO batteries, an optimal charging pattern can be proposed.

The advantages of the rule-based charging system lie in the ease of implementation. The charging station developer can predefine a set of rules based on changes in the climatic conditions, the nature of the user and their requirement for rapid charging, as well as the condition of the electric grid over a period of time. The charger should be designed to meet the

Table 4 Example rule set for charging: the set of rules is designed based on the results obtained for the selected battery in this work. The user selection is not demonstrated in the process when the grid is in peak load hours. Furthermore, frequency, the duty cycle of the pulses and the amplitude of the charge and discharge pulse should be either computed online *via* preset optimisation algorithms or set as a predefined value determined based on experiments/simulations for any charging technique (*CT5, CT9 or any pulse charging with discharge) defined in the table

No.	Present battery health	Environmental conditions	User requirement	Charging technique
1	New	Low	Rapid	Start charging with a high charge current pulse or pulse charging with discharge (similar to CT9*). With an increase in the internal cell temperature, a charge technique similar to CT5* can be used for rapid charging.
2	New	Normal	Rapid	Start charging with a charging technique similar to CT5*.
3	New	High	Rapid	Start charging with a technique similar to CT5* and monitor the internal temperature. With a rise in the internal cell temperature, C_{rate} should be reduced to constrain the rise. On stabilising the rise in internal cell temperature, C_{rate} can be increased again.
4	Half-life	Low	Rapid	Start charging using a technique similar to CT9*, with the amplitude of the discharge pulse lower than the average charge current. Monitor the rise in internal cell temperature. With the rise in internal cell temperature, shift charging to CT5. The internal cell temperature should be monitored to reduce C_{rate} on a rapid rise.
5	Half-life	Normal	Rapid	Start charging using a technique similar to CT5 while monitoring the internal cell temperature. An increase in the internal cell temperature near the stability limits should be constrained by reducing C_{rate}.
6	Half-life	High	Rapid	Start charging using a technique similar to CT5 and monitor the rise in internal temperature. Constrain the rise in the internal cell temperature by reducing C_{rate}. On decreasing and stabilising the internal cell temperature, C_{rate} can be increased.
7	Degraded	Low	Rapid	Start charging by deploying pulse charging with discharge with the amplitude of the discharge pulse higher than the average charge current. The rise in the internal cell temperature should be monitored. The charging should shift to a technique similar to CT5 with a rise in temperature. The internal cell temperature should be monitored and a reduction in C_{rate} should be used to constrain the rise.
8	Degraded	Normal	Rapid	The charging should be performed using a technique similar to CT5 and the internal cell temperature should be monitored. C_{rate} should be decreased to constrain the rise in internal cell temperature after a certain safe value.
9	Degraded	High	Rapid	The charging should start using a technique similar to CT5 and the internal cell temperature should be monitored. With an increase in the internal cell temperature above a certain safe value, C_{rate} should be reduced. The C_{rate} can be increased again once the cell reaches the level of a normal internal cell temperature.
10	New	Low	Slow	Start charging using a technique similar to pulse charging with discharge with the amplitude of the pulse discharge greater than the average charge current. The rise in temperature should be monitored, and if it increases, shift to a technique similar to CT5. The C_{rate} should be decreased if the rise in internal cell temperature is observed around stability limits.
11	New	Normal	Slow	A technique similar to CT5 should be used to charge, and regular monitoring of the rise in the internal cell temperature should be done. The rise in internal cell temperature near stability limits should be constrained by decreasing C_{rate}.
12	New	High	Slow	Start charging using a technique similar to CT5 and monitoring the rise in the internal cell temperature. Reduce the C_{rate} to control the rise in internal cell temperature.
13	Half-life	Low	Slow	The charging should start using pulse charging with discharge with an amplitude of the pulse discharge greater than the average charge current. The rise in internal cell temperature should lead to shifting to CT5 or CT8. Reduce C_{rate} to control the rise in the internal cell temperature.
14	Half-life	Normal	Slow	The charging should be done using a technique similar to CT5. The internal cell temperature should be monitored and C_{rate} should be changed to constrain the rise in the internal cell temperature.
15	Half-life	High	Slow	Start charging using a technique similar to CT5 and monitor the internal cell temperature. Modify C_{rate} to control the rise in the internal cell temperature.
16	Degraded	Low	Slow	Start charging using pulse charging with discharge with the amplitude of the discharge pulse higher than the average charge current. Monitor the rise in internal cell temperature, and shift charging to CT5 if the temperature rises. The internal cell temperature should be monitored and C_{rate} modified if it rises to around safety limits.
17	Degraded	Normal	Slow	A charging technique similar to CT5 should be performed with monitoring of the internal cell temperature. The C_{rate} should be modified to constrain the rise in internal cell temperature above safety limits.
18	Degraded	High	Slow	Start charging similar to CT5 and monitor the rise in internal cell temperature. With an increase in the internal cell temperature around safety limits, C_{rate} should be reduced and, on reaching a normal internal cell temperature, C_{rate} can be increased.

needs of different charging strategies. A set of rules can be framed and fed to the controller of the charger. Every time a user connects for charging, as per the requirements, the rule will ensure the best services for both the EV user and the electric grid. The assurance of the lowest battery degradation will be an advantage for the EV user, and the electric grid will have the lowest impact due to uncoordinated rapid charging.

The disadvantages of such rule-based charging are data requirements related to battery parameters that need to be considered for rapid charging with reduced battery degradation. Furthermore, robust communication needs to be established with the grid for real-time monitoring of the loading. The charger should also be capable of communicating with the EV battery BMS. A computational signal-processing board or connected infrastructure is also required to monitor and control the charging of EV batteries. These requirements make the charging systems costly, but an increase in cost will be compensated by avoiding battery ageing and losses to the power system operators due to uncoordinated charging. The benefits of Li-ion batteries and their wide application in EVs have driven research interests in meeting the challenges. All of the challenges in EVs converge on one aspect: battery degradation.

Fig. 6 presents two scenarios for battery charging. Fig. 6(a) presents a possible charging pattern when the EV battery is charging at a normal or high ambient temperature. Considering the electric grid condition to be at off-peak load hour, the user opts to charge at a higher C_{rate}. The application of high C_{rate} leads to an increase in the internal cell temperature. However, on reaching a certain limit of internal cell temperature rise, the C_{rate} is reduced to constrain battery degradation. With monitored steps of reduction in the C_{rate}, the internal cell temperature will start to fall. The C_{rate} can be increased again on reaching a lower limit of the internal cell temperature rise. These limits can be determined based on simulation experiments performed on the cell used in the EVs. Another scenario of charging at a very low temperature is depicted in Fig. 6(c). Pulse charging with discharge offers a possibility to increase the internal cell temperature. Hence, the charging starts at the higher C_{rate} using pulse charging with a discharge pattern. On reaching the normal ambient temperature conditions, the charging continues with normal pulse charging. The internal cell temperature is monitored to increase and decrease the C_{rate}. The proposed charging is not limited to the use of only pulse charging and pulse charging with discharge. Other suitable charging patterns for particular cell electrochemistry characteristics can be determined, which will help to reduce the degradation rate. Table 4 summarizes a rule base that is developed considering all the five input parameters, i.e., battery health, the user C_{rate} requirement, electric grid conditions, ambient temperature, and the rise in internal cell temperature.

4 Conclusions

This work shows that by developing a methodology of charging, the rate of degradation in the battery is constrained irrespective of extreme changes in the ambient temperature and the requirement of rapid charging by EV users. Insightful analysis is obtained by developing a set of simulation experiments that help to assess the impact on the causes and the rate of battery degradation that are due to changes in the charging technique used, the C_{rate}, the ambient temperature and the various parameters of a variants of pulse charging. Although the use of the proposed charging methodology requires pre-analysis of the battery that is to be charged at a charging station, if used by the charging service providers, based on the conclusions drawn in the Results and discussion sections, the proposed charging technique can help to reduce the overall capacity fading of the battery. Furthermore, the proposed charging technique also considers the condition of the electric grid (peak load, off-peak load hours) when deciding on the C_{rate} to charge the battery. Hence, the impact of charging on the electric grid is also reduced. The analysis also guides the selection of the charging technique for utilisation in high-energy or high-power applications at different ambient temperatures. On the basis of this extensive analysis, the insight developed not only proposes a battery-friendly charging technique but also develops a rational and new means of approaching the development of future charging techniques.

Author contributions

Bikash Sah and Praveen Kumar performed the conceptualisation of the research. Bikash Sah performed data curation, formal analysis, investigation, methodology, resources, software, visualization, writing – original draft, review and editing. Praveen Kumar performed supervision, validation and, writing – review and editing.

Conflicts of interest

There are no conflicts to declare.

Acknowledgements

Notes and references

1 G. E. Blomgren, *J. Electrochem. Soc.*, 2016, **164**, A5019.
2 D. Kushnir, *Curr. State Future Prospects*, 2015, 1–56.

3 N. Nitta, F. Wu, J. T. Lee and G. Yushin, *Mater. Today*, 2015, **18**, 252–264.

4 A. Masias, J. Marcicki and W. A. Paxton, *ACS Energy Lett.*, 2021, **6**, 621–630.

5 L. Ellingsen and C. Hung, *STUDY, European Parliament, Directorate General for Internal Policies, Policy Department for Structural and Cohesion Policies, Transport and Tourism*, 2018, **10**, 944056.

6 F. Conte, *e & i Elektrotechnik und Informationstechnik*, 2006, **123**, 424–431.

7 P. Keil, S. F. Schuster, J. Wilhelm, J. Travi, A. Hauser, R. C. Karl and A. Jossen, *J. Electrochem. Soc.*, 2016, **163**, A1872.

8 J. Vetter, P. Novák, M. R. Wagner, C. Veit, K.-C. Möller, J. Besenhard, M. Winter, M. Wohlfahrt-Mehrens, C. Vogler and A. Hammouche, *J. Power Sources*, 2005, **147**, 269–281.

9 M. R. Palacn, *Chem. Soc. Rev.*, 2018, **47**, 4924–4933.

10 X. Han, L. Lu, Y. Zheng, X. Feng, Z. Li, J. Li and M. Ouyang, *eTransportation*, 2019, **1**, 100005.

11 V. Etacheri, R. Marom, R. Elazari, G. Salitra and D. Aurbach, *Energy Environ. Sci.*, 2011, **4**, 3243–3262.

12 G. Sikha, B. N. Popov and R. E. White, *J. Electrochem. Soc.*, 2004, **151**, A1104.

13 P. Arora, R. E. White and M. Doyle, *J. Electrochem. Soc.*, 1998, **145**, 3647.

14 J. Liu, Q. Duan, M. Ma, C. Zhao, J. Sun and Q. Wang, *J. Power Sources*, 2020, **445**, 227263.

15 X.-G. Yang, Y. Leng, G. Zhang, S. Ge and C.-Y. Wang, *J. Power Sources*, 2017, **360**, 28–40.

16 A. S. Mussa, A. Liivat, F. Marzano, M. Klett, B. Philippe, C. Tengstedt, G. Lindbergh, K. Edström, R. W. Lindström and P. Svens, *J. Power Sources*, 2019, **422**, 175–184.

17 S. E. O'Kane, W. Ai, G. Madabattula, D. Alonso-Alvarez, R. Timms, V. Sulzer, J. S. Edge, B. Wu, G. J. Offer and M. Marinescu, *Phys. Chem. Chem. Phys.*, 2022, **24**, 7909–7922.

18 P. Ramadass, B. Haran, P. M. Gomadam, R. White and B. N. Popov, *J. Electrochem. Soc.*, 2004, **151**, A196.

19 J. S. Edge, S. O'Kane, R. Prosser, N. D. Kirkaldy, A. N. Patel, A. Hales, A. Ghosh, W. Ai, J. Chen and J. Jiang, *et al.*, *Phys. Chem. Chem. Phys.*, 2021, **23**, 8200–8221.

20 C. M. Snyder, The Rate Depedency of Li-ion Battery Degradation Mechanisms, Sandia national lab.(snl-nm), albuquerque, nm (united states) technical report, 2016.

21 A. Raj, M.-T. F. Rodrigues and D. P. Abraham, *J. Electrochem. Soc.*, 2020, **167**, 120517.

22 S. S. Zhang, *J. Power Sources*, 2006, **161**, 1385–1391.

23 G. Sikha, P. Ramadass, B. Haran, R. E. White and B. N. Popov, *J. Power Sources*, 2003, **122**, 67–76.

24 P. Ramadass, B. Haran, R. White and B. N. Popov, *J. Power Sources*, 2002, **112**, 606–613.

25 A. Tomaszewska, Z. Chu, X. Feng, S. O'Kane, X. Liu, J. Chen, C. Ji, E. Endler, R. Li, L. Liu, Y. Li, S. Zheng, S. Vetterlein, M. Gao, J. Du, M. Parkes, M. Ouyang, M. Marinescu, G. Offer and B. Wu, *eTransportation*, 2019, **1**, 100011.

26 J. Li, E. Murphy, J. Winnick and P. A. Kohl, *J. Power Sources*, 2001, **102**, 302–309.

27 S. Li, Q. Wu, D. Zhang, Z. Liu, Y. He, Z. L. Wang and C. Sun, *Nano Energy*, 2019, **56**, 555–562.

28 F. Savoye, P. Venet, M. Millet and J. Groot, *IEEE Trans. Ind. Electron.*, 2011, **59**, 3481–3488.

29 H. Lv, X. Huang and Y. Liu, *Ionics*, 2020, 1–22.

30 S. Li, Q. Wu, D. Zhang, Z. Liu, Y. He, Z. L. Wang and C. Sun, *Nano Energy*, 2019, **56**, 555–562.

31 P. H. Notten, J. O. het Veld and J. Van Beek, *J. Power Sources*, 2005, **145**, 89–94.

32 M. F. Hasan, C.-F. Chen, C. E. Shaffer and P. P. Mukherjee, *J. Electrochem. Soc.*, 2015, **162**, A1382.

33 X. Hu, Y. Zheng, X. Lin and Y. Xie, *IEEE Trans. Transport. Electrification*, 2020, **6**, 427–438.

34 L. Patnaik, A. Praneeth and S. S. Williamson, *IEEE Trans. Ind. Electron.*, 2018, **66**, 1059–1067.

35 L.-R. Chen, S.-L. Wu, D.-T. Shieh and T.-R. Chen, *IEEE Trans. Ind. Electron.*, 2012, **60**, 88–97.

36 Y. Lee and S. Park, *IEEE Trans. Power Electron.*, 2015, **30**, 4232–4243.

37 J. Chen, Y. Lee and S. Park, *2015 9th International Conference on Power Electronics and ECCE Asia (ICPE-ECCE Asia)*, 2015, pp. 2582–2589.

38 M. Bayati, M. Abedi, G. B. Gharehpetian and M. Farahmandrad, *IEEE Trans. Vehicular Technology*, 2020, **69**, 7201–7210.

39 H. Vazini, *IET Power Electronics*, 2019, **12**, 421–429(8).

40 Z. Zhang, Z. L. Wang and X. Lu, *Adv. Energy Mater.*, 2019, **9**, 1900487.

41 A. Bessman, R. Soares, S. Vadivelu, O. Wallmark, P. Svens, H. Ekström and G. Lindbergh, *IEEE Trans. Ind. Electron.*, 2018, **65**, 4750–4757.

42 X. Lin, X. Hao, Z. Liu and W. Jia, *J. Power Sources*, 2018, **400**, 305–316.

43 H. Perez, S. Dey, X. Hu and S. Moura, *J. Electrochem. Soc.*, 2017, **164**, A1679.

44 S. Pramanik and S. Anwar, *J. Power Sources*, 2016, **313**, 164–177.

45 T. Waldmann, M. Kasper and M. Wohlfahrt-Mehrens, *Electrochim. Acta*, 2015, **178**, 525–532.

46 F. B. Spingler, W. Wittmann, J. Sturm, B. Rieger and A. Jossen, *J. Power Sources*, 2018, **393**, 152–160.

47 S. Schindler, M. Bauer, H. Cheetamun and M. A. Danzer, *J. Energy Storage*, 2018, **19**, 364–378.

48 C. Zou, X. Hu, Z. Wei, T. Wik and B. Egardt, *IEEE Trans. Ind. Electron.*, 2017, **65**, 6635–6645.

49 M. Song and S.-Y. Choe, *J. Power Sources*, 2019, **436**, 226835.

50 K. Liu, X. Hu, Z. Yang, Y. Xie and S. Feng, *Energy Convers. Manage.*, 2019, **195**, 167–179.

51 J. Zhu, M. S. Dewi Darma, M. Knapp, D. R. Sørensen, M. Heere, Q. Fang, X. Wang, H. Dai, L. Mereacre, A. Senyshyn, X. Wei and H. Ehrenberg, *J. Power Sources*, 2020, **448**, 227575.

52 J. Cao, D. Harrold, Z. Fan, T. Morstyn, D. Healey and K. Li, *IEEE Trans. Smart Grid*, 2020, **11**, 4513–4521.

53 E. J. Dickinson and A. J. Wain, *J. Electroanal. Chem.*, 2020, **872**, 114145.

54 A. Seaman, T.-S. Dao and J. McPhee, *J. Power Sources*, 2014, **256**, 410–423.

55 M. Doyle, T. F. Fuller and J. Newman, *J. Electrochem. Soc.*, 1993, **140**, 1526.

56 C. M. Doyle, *Design and simulation of lithium rechargeable batteries*, PhD thesis, 1995.

57 S. G. Marquis, V. Sulzer, R. Timms, C. P. Please and S. J. Chapman, *J. Electrochem. Soc.*, 2019, **166**, A3693.

58 R. Timms, S. G. Marquis, V. Sulzer, C. P. Please and S. J. Chapman, *SIAM J. Appl. Math.*, 2021, **81**, 765–788.

59 V. Sulzer, S. G. Marquis, R. Timms, M. Robinson and S. J. Chapman, *J. Open Res. Software*, 2021, **9**, 14.

60 V. R. Subramanian, V. D. Diwakar and D. Tapriyal, *J. Electrochem. Soc.*, 2005, **152**, A2002.

61 R. Deshpande, M. Verbrugge, Y.-T. Cheng, J. Wang and P. Liu, *J. Electrochem. Soc.*, 2012, **159**, A1730.

62 S. G. Marquis, R. Timms, V. Sulzer, C. P. Please and S. J. Chapman, *J. Electrochem. Soc.*, 2020, **167**, 140513.

63 M. Safari, M. Morcrette, A. Teyssot and C. Delacourt, *J. Electrochem. Soc.*, 2008, **156**, A145.

64 Q. Liu, C. Du, B. Shen, P. Zuo, X. Cheng, Y. Ma, G. Yin and Y. Gao, *RSC Adv.*, 2016, **6**, 88683–88700.

65 D. Zhang, B. Haran, A. Durairajan, R. E. White, Y. Podrazhansky and B. N. Popov, *J. Power Sources*, 2000, **91**, 122–129.

66 P. Keil and A. Jossen, *J. Energy Storage*, 2016, **6**, 125–141.

67 Y. Liu, Y. Zhu and Y. Cui, *Nat. Energy*, 2019, **4**, 540–550.

68 B. Balagopal and M.-Y. Chow, *Batteries*, 2020, **6**, 53.

69 M. H.-M. Tang, PhD thesis, UC Berkeley, 2012.

70 X. Zhang, A. M. Sastry and W. Shyy, *J. Electrochem. Soc.*, 2008, **155**, A542.

71 S. Pelletier, O. Jabali, G. Laporte and M. Veneroni, *Trans. Res., Part B: Methodological*, 2017, **103**, 158–187.

72 L. Lu, X. Han, J. Li, J. Hua and M. Ouyang, *J. Power Sources*, 2013, **226**, 272–288.

73 R. Xiong, Y. Pan, W. Shen, H. Li and F. Sun, *Renewable Sustainable Energy Rev.*, 2020, **131**, 110048.

74 D. H. Doughty and C. C. Crafts, FreedomCAR: electrical energy storage system abuse test manual for electric and hybrid electric vehicle applications, Sandia national laboratories technical report, 2006.

75 X. Zhou, J. Huang, Z. Pan and M. Ouyang, *J. Power Sources*, 2019, **426**, 216–222.

76 A. Andersson and K. Edström, *J. Electrochem. Soc.*, 2001, **148**, A1100.

77 M. Richard and J. Dahn, *J. Electrochem. Soc.*, 1999, **146**, 2068.

78 H. Maleki, G. Deng, A. Anani and J. Howard, *J. Electrochem. Soc.*, 1999, **146**, 3224.

79 D. MacNeil, D. Larcher and J. Dahn, *J. Electrochem. Soc.*, 1999, **146**, 3596.

80 P. Arora, M. Doyle and R. E. White, *J. Electrochem. Soc.*, 1999, **146**, 3543.

81 C.-K. Huang, J. Sakamoto, J. Wolfenstine and S. Surampudi, *J. Electrochem. Soc.*, 2000, **147**, 2893.

82 L.-R. Chen, *IEEE Trans. Ind. Electron.*, 2007, **54**, 398–405.

83 B. Sah, P. Kumar, R. Rayudu, S. K. Bose and K. P. Inala, *IEEE Trans. Ind. Inform.*, 2018, **15**, 3923–3933.

84 B. Sah, P. Kumar and S. K. Bose, *IEEE Syst. J.*, 2021, **15**, 3301–3311.

85 M. Muratori, *Nat. Energy*, 2018, **3**, 193–201.

86 A. Thingvad, L. Calearo, P. B. Andersen and M. Marinelli, *IEEE Trans. Vehicular Technol.*, 2021, **70**, 7547–7557.